Electronic structure of MnSi: The role of electron-electron interactions

F. Carbone,[1] M. Zangrando,[2] A. Brinkman,[1] A. Nicolaou,[2] F. Bondino,[2] E. Magnano,[2] A. A. Nugroho,[4,5] F. Parmigiani,[2,3] Th. Jarlborg,[1] and D. van der Marel[1]

[1]*Département de Physique de la Matière Condensée, Universitée de Genève, CH-1211 Genève 4, Switzerland*
[2]*Laboratorio Nazionale TASC-CNR, Basovizza Strada Statale 14, Km 163.5, 34012 Trieste, Italy*
[3]*INFM, Dipartimento di Matematica e Fisica, UCSC, Via dei Musei 41, 25121 Brescia, Italy*
[4]*Materials Science Centre, University of Groningen, 9747 AG Groningen, The Netherlands*
[5]*Jurusan Fisika, Institut Teknologi Bandung, Indonesia*

We present an experimental study of the electronic structure of MnSi. Using x-ray absorption spectroscopy (XAS), x-ray photoemission, and x-ray fluorescence, we provide experimental evidence that MnSi has a mixed valence ground state. We show that self-consistent local density approximation supercell calculations cannot replicate the XAS spectra of MnSi, while a good match is achieved within the atomic multiplet theory assuming a mixed valence ground state. We discuss the role of the electron-electron interactions in this compound and estimate that the valence fluctuations are suppressed by a factor of 2.5, which means that the Coulomb repulsion is not negligible.

PACS number(s): 71.27.+a, 75.25.+z, 75.10.−b, 78.70.Dm

Traditionally, the magnetism of MnSi is considered as weakly itinerant,[1,2] i.e., the spin polarization is modeled as a relative shift of bands of delocalized Bloch states for the two spin directions. At ambient pressure, MnSi orders helimagnetically below $T_C = 29.5$ K, and becomes ferromagnetic in a magnetic field exceeding 0.6 T. The Hall effect and the negative magnetoresistance[3] in the ferromagnetic phase agree well with the theory of spin fluctuations in itinerant ferromagnetism.[1] Also the inelastic neutron scattering data can be interpreted in this framework.[4] The saturation moment of the magnetically ordered phase is $0.4\mu_B$ per Mn atom. On the other hand, *ab initio* calculations based on the the local density approximation (LDA) indicate a tendency of the Mn atoms to form a moment close to $1\mu_B$ if the real lattice constant for MnSi (4.558 Å) is used.[5,6] A fit of the susceptibility in the paramagnetic phase to a Curie-Weiss law gives $2.2\mu_B$ per Mn atom.[7]

Recently, several properties of MnSi have been discovered which had not been anticipated on the basis of the itinerant model and which remain to be fully understood: Above 14.6 kbar, the material enters a phase with partial helimagnetic order along the $(1,1,0)$ direction,[8] where the electrical resistivity is proportional to $T^{3/2}$ in contradiction to standard notions of a Landau Fermi liquid.[9] A further indication of anomalous low energy scale properties follows from the non-Drude infrared optical conductivity at ambient pressure,[10] proportional to $(i\omega)^{-1/2}$. Above T_C, the resistivity is described by the formula[10] $\rho = \rho_{sat} T/(T_0 + T)$ which for $T \gg T_0 = 180$ K approaches the Mott-Ioffe-Regel limit, $\rho_{sat} = 287$ $\mu\Omega$ cm. The rapid rise toward saturation corresponds to a strong dissipation of the charge transport. The abrupt drop of the electrical resistivity when the material is cooled through T_C suggests that this dissipation is due to a coupling to magnetic fluctuations.

Here, using x-ray Absorption Spectroscopy (XAS), x-ray photoelectron spectroscopy (XPS), and x-ray fluorescence spectroscopy (XFS), we provide the experimental evidence

that MnSi has a mixed valence ground state which cannot be described by the standard LDA approach. We will show that the electron-electron correlations are not negligible, the value of U/W is estimated to be around 0.4, where U is the on-site Coulomb repulsion and W is the bandwidth; we think that most likely the observed deviations from the usual itinerant picture are due to the suppression of valence fluctuations in the ground state of the material.

The crystal structure of MnSi is generated by the cubic $B20$ structure.[11,12] The unit cell contains 4 Mn atoms at crystallographically equivalent positions. The sublattice of the transition metal atoms, displayed in Fig. 1, reveals that the basic structural element is an equilateral triangle of three Mn atoms. The structure is a corner-sharing one: Each Mn atom connects three triangles, which occur with four different orientations along the body diagonals of the cubic unit cell. The singly connected loops of the structure shown in Fig. 1 contain an odd number of bonds. The structural similarity to the pyrochlore,[13,14] Kagome,[15,16] gadolinium gallium garnet,[17] and the β-Mn lattices[18,19] is a peculiarity that has been overlooked so far and that might play a role in the formation of the helical magnetic structure observed below 29 K.

MnSi high quality single crystals were grown by the floating zone technique starting from $4N$ purity Mn and $5N$ purity Si. All samples were characterized by x-ray diffraction, energy dispersive x-ray (EDX) elemental analysis and electrical resistivity. The residual resistivity of all MnSi samples was less than 2 $\mu\Omega$ cm.

The experiments were performed at the BACH beam line[20] of the ELETTRA synchrotron in Trieste. XAS was performed in total electron yield (TEY), measuring roughly the first 50 Å of the surface, and total fluorescence yield (TFY), measuring down to 200 nm in the bulk. The XAS spectra were normalized to the incident photon flux, the resolution in TEY was 150 meV and 400 meV in TFY. The fluorescence experiments were done recording the fluorescent decay of Mn $3d \rightarrow 2p$ and $2p \rightarrow 3s$ levels on a charge-coupled device (CCD) detector.
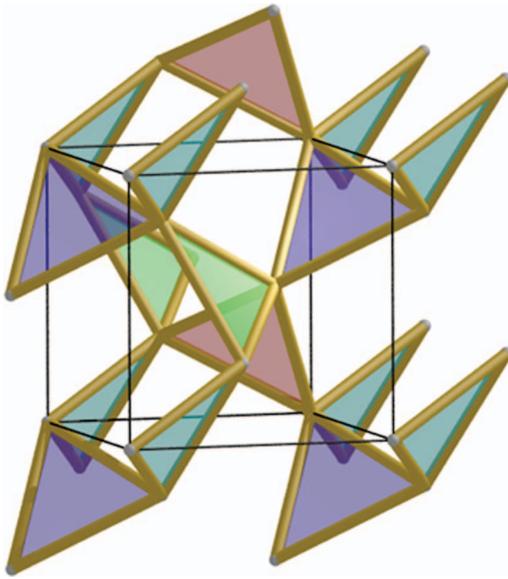
FIG. 1. (Color) Mn sublattice of MnSi. The corners of the triangles, all of which are equilateral, correspond to the positions of the Mn atoms.

Large single crystals were cleaved *in situ* prior to the measurements in order to obtain clean surfaces; the surface quality was checked with XPS, Fig. 2. The base pressure in the measurement chamber was 1×10^{-10} mbar. XAS and XPS spectra were recorded at room temperature within minutes after cleaving. The contamination of the surface before
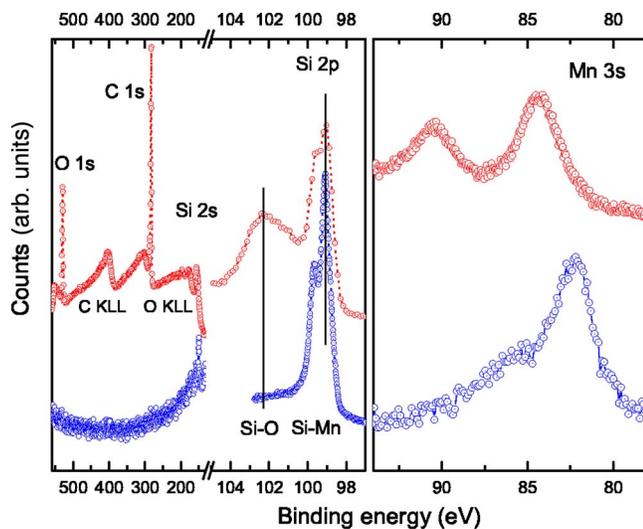

FIG. 2. (Color online) XPS spectra of MnSi before and after cleaving. In the right part of the figure, one can see the high resolution spectra of the Mn $3s$ levels measured with an incident photon energy of 418 eV and the Si $2p$ levels measured with an incident photon energy of 196 eV before cleaving and 142 eV after cleaving; in the left part, a survey from the Si $2s$ to the O $1s$ is displayed measured at 655 eV incident photon energy. The blue curve represents the spectrum after cleaving, the red curve was recorded before cleaving. After cleaving, the high binding energy component of the Si $2p$ line is suppressed, the Mn $3s$ level splitting diminishes, and the C and O $1s$ lines are also suppressed.
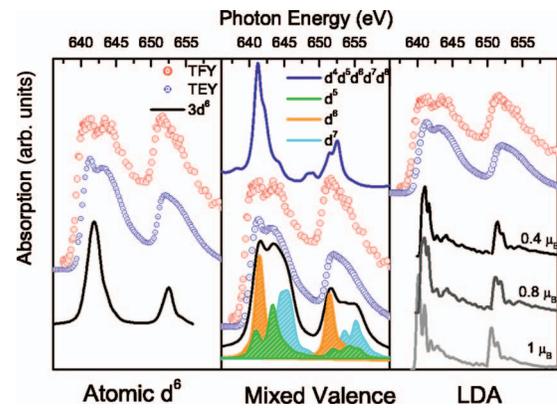

FIG. 3. (Color) Left panel: Mn $L_{2,3}$ edge measured XAS together with atomic multiplet calculation for a $3d^6$ ground state. The TFY experiment has a resolution of 0.4 eV (red open symbols); the TEY experiment has a resolution of 0.2 eV (blue open symbols). Middle panel: The experimental spectra are plotted together with the Mn mixed valence atomic multiplets calculations in a cubic crystal field (black line); below this line is possible to see the contribution from the different configurations. The dark blue line represents the superposition of the d^4, d^5, d^6, and d^7 configurations with the weights given by the binomial distribution in Table I, which corresponds to the noninteracting particle picture. Right panel: The LDA calculations are plotted for three different values of the lattice parameter together with the experimental spectra.

and after cleaving was checked by oxygen and carbon $1s$ photoemission. The cleaved surface of the sample was scanned spatially with steps of 100 μm and XPS was recorded at each position. This analysis showed that a significant carbon contamination is present on the border of the sample. This contamination affects dramatically the shape of the TEY XAS. Only at least 150 μm away from the sample's border, where the XPS reveals a very clean surface, we could have a TEY spectrum in agreement with the TFY one, representative of the bulk properties of the material. In the XPS spectra, recorded in the middle of a cleaved sample, the oxygen and carbon $1s$ lines are completely suppressed with respect to the noncleaved sample, as shown in Fig. 2. The analysis of the surface revealed that carbon, MnO, and SiO_2 are the main contaminants. The XPS of Si $2p$ levels shows a component around 102 eV associated to SiO_2; the Mn $3s$ splitting on the sample before cleaving was 6.3 eV, in agreement with earlier reports for MnO.[21] In the cleaved sample, the high binding energy peak of the Si $2p$ level is suppressed, the Mn $3s$ levels splitting diminishes to a much smaller value and the carbon and oxygen $1s$ lines are suppressed.

In Fig. 3, we display the Mn $L_{2,3}$ XAS spectrum of MnSi measured both in TEY and TFY; one can see that the two spectra are almost identical, indicating that we are probing, indeed, the bulk. The two main peaks correspond to the $2p_{1/2}$ (642 eV) and $2p_{3/2}$ (653 eV) spin-orbit split components of the $2p$ core level. In a one-particle picture, these two edges have the same spectral shape, as illustrated by a first principles calculation using the LDA (black line in Fig. 3). Self-consistent (LDA-LMTO) LDA linear muffin tin orbital calculations have been performed for 64-atom supercells; one of the Mn atoms has a core hole. The ground state of the
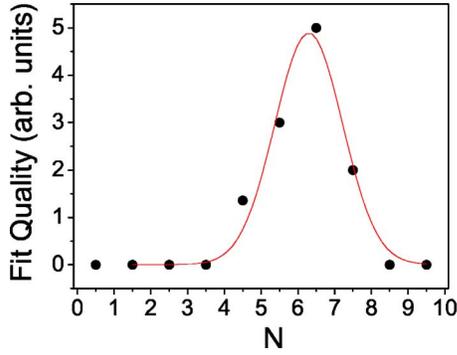
FIG. 4. (Color online) We display the inverse χ^2 for the fits to the experimental data of the superposition of d^4+d^5, d^5+d^6, d^6+d^7, and d^7+d^8, respectively.

calculation was ferromagnetic, adopting three different states of magnetic polarization characterized by local moments of 0.4, 0.8, and $1\mu_B$, labeled as such in Fig. 3. The XAS spectrum corresponds to a broadened sum of the unoccupied local spin Mn-d density of states (DOS) functions. A known problem of band calculations in MnSi is the predicted value of the local moment on the transition metal atom.[6] This quantity is strongly dependent on the unit cell dimension and tends to be higher then the measured one when the lattice constant has the experimentally determined dimension of 4.558 Å. We checked the influence of this effect on the XAS spectrum in three cases, changing the lattice constant: the local moment of Mn is $0.4\mu_B$ (the experimentally measured value) for a lattice parameter $a=4.36$ Å, 0.8 for $a=4.5$ Å, and $1\mu_B$ for the measured lattice constant $a=4.55$ Å. This is shown in the right panel of Fig. 3; this effect weakly modifies the XAS spectrum and cannot explain the strong departure from the measured one. It is evident that LDA calculations are narrower and cannot replicate the XAS spectra for MnSi. In the middle panel of Fig. 3, we also compare the experimental spectra with atomic model calculations performed with a standard computer program.[22] We calculate the XAS spectra for several different configurations: Mn $3d^4$, $3d^5$, $3d^6$, $3d^7$, and d^8 in a cubic crystal field environment of 2.4, 2.6, and 3 eV. Furthermore, least-mean-squares fits to the data of the weighted superposition of four single valence spectra, d^4, d^5, d^6, d^7 and d^5, d^6, d^7, d^8, were performed. The least-mean-squares routine tends to give a negligible weight to the d^4 and d^8 configurations. We estimate the error bars of this approach as the maximum spread of values obtained for the d^5, d^6, d^7 configurations in the two cases for the three mentioned values of the crystal field. The crystal field is estimated from the band splitting observed in the high symmetry points of the band calculations.[5] In the best fit, the relative weights of the different valences are found to be 0% d^4, 21% d^5, 55% d^6, 24% d^7, and 0% d^8 in a crystal field of 2.6 eV. In Fig. 4, we also plot the inverse of the χ^2 obtained fitting the experimental data to the combination of d^4+d^5, d^5+d^6, d^6+d^7, and d^7+d^8, respectively. This calculation shows that the fitting quality is peaked around the d^6 configuration and supports the conclusion that a large contribution to the XAS spectrum comes from the $3d^6$ configuration.

In the left panel of Fig. 3, we also show a calculation for

TABLE I. Theoretical $P(N)$ assuming noninteracting particles, $[P_{NI}(N)]$, experimental $P(N)$ obtained from the mixed-valence fit to the XAS spectrum, $[P_{exp}(N)]$. The values of $\Delta(N)$ correspond to the shift of the energies $E(2p \rightarrow 3d^{N+1})$, with respect to the output of the Cowan code, of the final state multiplets; the cubic crystal field parameter was 2.6 eV for all configurations.

N	$P_{NI}(N)$	$P_{exp}(N)$	$\Delta(N)$
0	0.0001		
1	0.0015		
2	0.011		
3	0.042		
4	0.111		
5	0.193	0.21	2
6	0.251	0.55	0.38 eV
7	0.215	0.24	3.72 eV
8	0.121		
9	0.04		
10	0.006		

an atomic $3d^6$ ground state; this simple calculation also does not represent satisfactorily the experiments. The better agreement between the experiments and the atomic multiplet mixed valence calculation emphasizes two important properties of the electronic configuration of MnSi: (i) the dominant configuration is $3d^6$; (ii) experimentally, the valence fluctuations are given by

$$p(N) = P(N_0)\exp\left[-\left(\frac{N-N_0}{\delta N}\right)^2\right], \quad (1)$$

where $\delta N_{exp}=0.92$ and $N_0=6$. For noninteracting particles distributed over 10 3d bands, having the average occupation of six electrons ($N_0=6$), $P(N)$ is given by the binomial equation

$$P_{NI}(N) = 0.6^N 0.4^{10-N} 10! \frac{N!}{N!(10-N)!} \quad (2)$$

(NI=noninteracting), which is to a very good approximation given by Eq. (1) with $N_0=6$ and $\delta N_{NI}=2.25$. Thus the value $\delta N_{NI}/\delta N_{exp}=2.5$ gives a measure of the valence suppression in the ground state. In Table I, we show the probability of having N electrons on an ion as a function of the occupation number in a LDA picture, together with the experimental findings. In Fig. 5, one can see the fit to Eq. (1) for the experimentally derived $P(N)$ and the theoretical ones. The sharp suppression of valence fluctuations in the ground state of Mn observed experimentally is likely the consequence of the on-site Coulomb interaction in the 3d shell of Mn. For the d^6 configuration of Mn $U_{eff}=F_0-J-C=1$ eV,[23] where F_0 is the intrashell Coulomb repulsion, J is the intrashell exchange interaction, and C takes into account all the multipole contributions of the Coulomb and exchange interactions. The overall 3d bandwidth of MnSi is about 6 eV, but this value in part reflects a relative shift of the different group of bands, representing the crystal field splitting. The
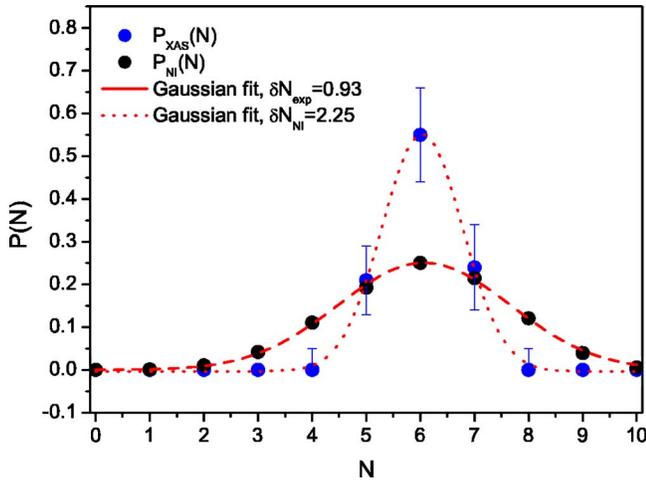
FIG. 5. (Color online) The theoretical and experimentally derived values of $P(N)$ are plotted together with the fit to Eq. (1). From these fits, we extract the values for δN and thus $\delta N_{NI}/\delta N_{exp}$ =2.5.

width of each of the subbands is approximatively 2.5 eV, hence $U=0.4$ W in this compound. This value implies that MnSi has to be considered as an itinerant system. On the other hand, the valence fluctuations should be strongly suppressed as compared to the noninteracting picture, and this indeed corresponds to what we observed experimentally.

In Fig. 6, we present the photoemission spectrum of the Mn $3s$ core level measured at an incident photon energy of 418 eV and the fluorescence spectrum measured at a photon energy of 660 eV; since photoemission is a very surface sensitive technique, we cross-check our results acquiring the corresponding fluorescence spectrum when possible. The Mn $3s$ photoemission shows a shoulder on the high energy side of the spectrum. Most likely, the mixed valence ground state we discussed before is responsible for this weak shoulder visible in the $3s$ spectrum. The asymmetry of the $3s$ levels
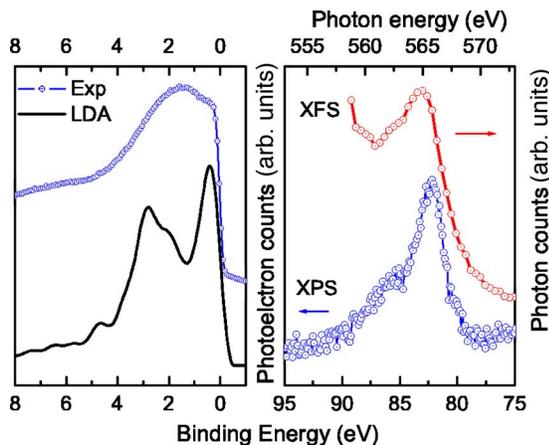

FIG. 6. (Color online) Top panel: VB photoemission measured at an incident photon energy of 104 eV together with LDA calculations. Lower panel: Photoemission (blue open symbols) measured at 418 eV incident photon energy and fluorescent (red open symbols) spectra of Mn $3s$ levels measured at 660 eV incident photon energy.

photoemission in insulating Mn compounds, such as MnO, MnF_2, or manganites, has been shown to be caused by the many-body interaction between the core-hole electron and the localized $3d$ electrons.[21,24] In this case the role of the exchange interaction is predominant and, when the orbital moment does not contribute to the total magnetic moment of the charge carriers, a direct relation between the $3s$ level splitting and the spin magnetic moment is valid. On the other hand, it is well known that this relation does not hold any longer in more metallic systems.[25] When the electronegativity of the ligand atom decreases, the charge transfer satellites and the screening of the final state become more important; as a result, it is not possible any longer to attribute the peaks in the $3s$ spectra to pure spin states. Usually, in more covalent systems, the $3s$ levels splitting is smaller than what one would expect in the localized scenario because of these effects. We believe that this is the case in MnSi, whose metallic behavior reflects the covalent nature of the Mn-Si bonding.

In Fig. 6, we also compare the experimental valence band photoemission spectra with the LDA calculations. The calculations include the radial matrix elements but ignore the k conservation between initial and final states. This is a reasonable approximation in the limit of large photon energy.[26] In the calculation, a peak is evident around 2.8 eV away from the Fermi edge, a similar feature is visible in the experimental spectrum, although its position is only 1.8 eV away from the Fermi edge. The valence band (VB) photoemission spectra have been collected using three incoming photon energies: 86 eV, 104 eV, and 196 eV and no appreciable changes where observed. Also in this case, the agreement between the calculation and the experiment is not satisfactory. The valence band photoemission on MnSi has already been reported together with the LDA calculation in Ref. 27. The authors point out that the major deviations from the raw spectra and the calculations are ascribable to the on-site Coulomb repulsions, in agreement with our conclusion.

Our observations evidence the fact that in this class of materials it is not justified to neglect completely the electron-electron correlations. The discrepancy between the single particle scenario and the experiment is corroborated by the comparison in Fig. 3(a) of the LDA prediction of the XAS spectrum to the experimental data. It would be tempting to attribute this discrepancy to the fact that XAS is a high energy probe, and that the observed spectra correspond to the final state with an extra core-hole present. However, (i) both in the band calculation as well as in the atomic multiplet calculations shown in Fig. 3(a), the presence of the core hole has been taken into account, (ii) theoretically these spectra are expected to be a very sensitive fingerprint of the initial state electronic configuration, (iii) the same concerns would apply to the transition metal oxide family, where XAS has been quite successful in probes of the magnetic properties.[28–31] Moreover, also valence band photoemission, where no core hole is present, is inconsistent with the LDA approach. The cross-check of the results by means of different techniques, electron counting and photon counting techniques, makes us confident that we are indeed probing the electronic structure of bulk MnSi. Our estimated value for U/W around 0.4 classifies MnSi in a class of materials where

none of the two approximations is particularly good: completely neglecting the electron-electron interactions or considering them as dominant. The helical magnetic structure of MnSi has been explained in terms of the Dyaloshinskii-Moryia interaction; the interplay between spin-orbit coupling and exchange interaction can result in an anisotropic exchange interaction, responsible for the helical magnetic structure in low symmetry crystals. For this to happen, the motion of the conduction electrons must have a finite orbital component, for example, a $3d^5(^6S)$ ground state would be rather unfavorable in this context, having a null orbital moment. Our observations are compatible with this picture, providing an experimental support to the microscopic model.

In conclusion, we examined the electronic structure of MnSi using XAS, XFS, and XPS. The experimental data indicate that MnSi has a mixed-valence ground state of predominantly $3d^6$ character. The suppression of the valence fluctuations indicate that a considerable electron-electron interaction is present in this material; we estimate that the valence fluctuations are suppressed by a factor of 2.5, meaning that the Coulomb repulsions are non-negligible, but insufficient to form local moments on the Mn $3d$ shell.

[1] T. Moriya and A. Kawabata, J. Phys. Soc. Jpn. **34**, 639 (1973).

[2] L. Taillefer, G. G. Lonzarich, and P. Strange, J. Magn. Magn. Mater. **54-57**, 957 (1986).

[3] N. Manyala, Y. Sidis, J. F. di Tusa, G. Aeppli, D. P. Young, and Z. Fisk, Nature (London) **404**, 581 (2000).

[4] Y. Ishikawa, Y. Noda, Y. J. Uemura, C. F. Majkrzak, and G. Shirane, Phys. Rev. B **31**, 5884 (1985).

[5] T. Jeong and W. E. Pickett, Phys. Rev. B **70**, 075114 (2004).

[6] P. Lerch and Th. Jarlborg, J. Magn. Magn. Mater. **131**, 321 (1994).

[7] J. H. Wernick, G. K. Wertheim, and R. C. Sherwood, Mater. Res. Bull. **7**, 1153 (1972).

[8] C. Pfleiderer, D. Reznik, L. Pintschovius, H. v. Lohneysen, M. Garst, and A. Rosch, Nature (London) **427**, 15 (2004).

[9] N. Doiron-Leyraud, I. R. Walker, L. Taillefer, M. J. Steiner, S. R. Julian, and G. G. Lonzarich, Nature (London) **425**, 595 (2003).

[10] F. P. Mena, D. van der Marel, A. Damascelli, M. Fath, A. A. Menovsky, and J. A. Mydosh, Phys. Rev. B **67**, 241101(R) (2003).

[11] B. Borén, Ark. Kemi, Mineral. Geol. **11A**, 1 (1933).

[12] D. van der Marel, A. Damascelli, K. Schulte, and A. A. Menovsky, Physica B **244**, 138 (1998).

[13] X. Obradors, A. Labarta, A. Isalgue, J. Tejada, J. Rodriguez, and M. Pernet, Solid State Commun. **65**, 189 (1988).

[14] A. P. Ramirez, G. P. Espinosa, and A. S. Cooper, Phys. Rev. Lett. **64**, 2070 (1990).

[15] C. Broholm, G. Aeppli, G. P. Espinosa, and A. S. Cooper, Phys. Rev. Lett. **65**, 3173 (1990).

[16] J. T. Chalker, P. C. W. Holdsworth, and E. F. Shender, Phys. Rev. Lett. **68**, 855 (1992).

[17] P. Schiffer, A. P. Ramirez, D. A. Huse, P. L. Gammel, U. Yaron, D. J. Bishop, and A. J. Valentino, Phys. Rev. Lett. **74**, 2379 (1995).

[18] H. Nakamura, K. Yoshimoto, M. Shiga, M. Nishi, and K. Kakurai, J. Phys.: Condens. Matter **9**, 4701 (1997).

[19] B. Canals and C. Lacroix, Phys. Rev. B **61**, 11251 (2000).

[20] M. Zangrando, M. Finazzi, G. Paolucci, B. Diviacco, R. P. Walker, D. Cocco, and F. Parmigiani, Rev. Sci. Instrum. **72**, 1313 (2001).

[21] V. R. Galakhov, M. Demeter, S. Bartkowski, M. Neumann, N. A. Ovechkina, E. Z. Kurmaev, N. I. Lobachevskaya, Y. M. Mukovskii, J. Mitchell, and D. L. Ederer, Phys. Rev. B **65**, 113102 (2002).

[22] R. D. Cowan, *The Theory of Atomic Structure and Spectra* (University of California Press, Berkeley, 1981).

[23] D. van der Marel and G. A. Sawatzky, Phys. Rev. B **37**, 10674 (1988).

[24] L. Sangaletti, F. Parmigiani, and P. S. Bagus, Phys. Rev. B **66**, 115106 (2002).

[25] Gey-Hong Gweon, Je-Geun Park, and S. J. Oh, Phys. Rev. B **48**, 7825 (1993).

[26] T. Jarlborg and P. O. Nilsson, J. Phys. C **12**, 265 (1979).

[27] J. Y. Son, K. Okazaki, T. Mizokawa, A. Fuimori, T. Kanomata, and R. Note, J. Phys. Soc. Jpn. **71**, 1728 (2002).

[28] B. T. Thole, R. D. Cowan, G. A. Sawatzky, J. Fink, and J. C. Fuggle, Phys. Rev. B **31**, 6856 (1985).

[29] G. van der Laan and B. T. Thole, Phys. Rev. B **43**, 13401 (1991).

[30] B. T. Thole, P. Carra, F. Sette, and G. van der Laan, Phys. Rev. Lett. **68**, 1943 (1992).

[31] P. Carra, B. T. Thole, M. Altarelli, and X. Wang, Phys. Rev. Lett. **70**, 694 (1993).